Magnetic properties of nanocrystalline materials for high frequency applications

Craus, Cristian

Chapter 2

Experimental methods

In this chapter we describe the experimental methods. The synthesis of the samples is presented first, and then the basics of the analyzing techniques are explained. Special attention is given to the frequency-dependent permeability setup, which is especially developed for the research presented in this thesis.

2.1. Sample preparation

In this work we have used two synthesis methods: cold rolling and sputter deposition. Depending on the method, the nanocrystalline structure was obtained during sample production or after subsequent thermal treatments. The results, especially from the point of view of magnetic properties, will be presented in this thesis. Here, the basic aspects of the sample preparation are given.

2.1.1. Cold Rolling procedure

Cold rolling is a process by which a metal sheet is introduced between two rollers and then compressed and squeezed, see Fig. 2.1. Such treatment can result in useful combinations of mechanical properties like hardness, strength, ductility and others. However, in our case the main purpose for the sample preparation was the thickness reduction. The sheets used for rolling were cut from pure ingots of Fe-Ni-Cr, Fe-Ni-Ti and Fe-Ni-Si. An easy handling of the samples was obtained by placing them between two stainless-steel sheets. The sandwich was passed a few times between the rotating cylinders keeping the distance between the cylinders constant. The rolling was continued after changing slightly the distance between the cylinders. When the sample surface exceeded half of the stainless-steel sheets, the sample was cut in two. Only one piece was used for further reduction. Prior to this the sample was rotated by 90° with respect to the previous orientation; also the stainless-steel sheets were changed with new ones. The procedure was repeated until the desired thickness was obtained. A reduction of more than 99% was achieved for foils of 1 to 16 μm.

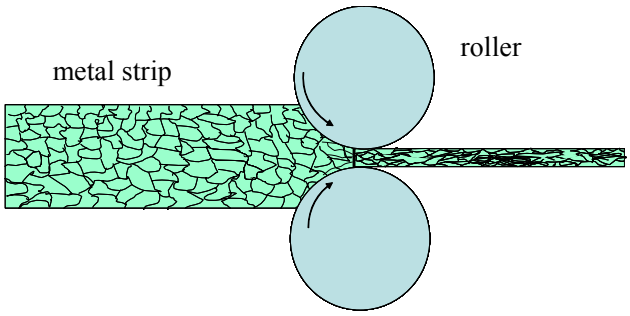

Fig. 2.1 The cold rolling process.

2.1.2. Reactive sputtering

Sputtering is a deposition technique used in a large range of functional applications [1] like synthesis of thin films or nanostructures. The process consists in bombarding a target (cathode) by energetic positive ions extracted from a glow discharge plasma placed in the proximity. In order to realize the extraction of the positive ions a negative potential is applied on the target. As a consequence of the collision of the positive ions with the target, atoms from the target are removed and will condensate on the substrate, forming a thin film. If the potential applied on the cathode is constant then the process is called DC sputtering.

The flux of the sputtered atoms or the deposition rate is proportional to the ionization efficiency, i.e. the density of the plasma. A dense plasma can be obtained if one uses a magnetic field parallel to the surface of the target. The magnetic field traps the electrons in helical trajectories which leads to a substantial increase of the occurrence of ionizing electron-ion collisions. Usually, when a magnetic field is present, this is indicated by using the term "magnetron". If in addition to the inert gas (Ar in our case) the sputtering atmosphere contains a reactive a reactive component (e.g. N_2 or O_2) the process is called reactive sputtering. Therefore the complete name of the technique used by us is DC reactive magnetron sputtering.

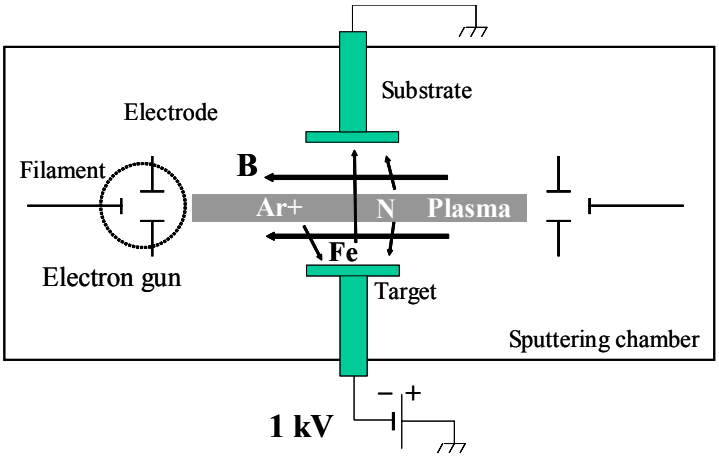

Fig. 2.2 Schematic representation of the sputtering apparatus

The sputtered films investigated in this thesis have been produced using the device presented in Fig. 2.2. Two electron guns (filaments) are used to ignite and control the density of the plasma. Consequently, a high sputtering rate (2-6 Å/s) can be obtained at a relatively low pressure (10^{-3} mbar). This design was optimized so that

we can sputter magnetic materials. In most commercial DC sputtering devices this is impossible because the magnet field is disturbed by the magnetisation of the target material.

In a typical deposition experiment, the sputtering chamber is first evacuated to a pressure of better than $1x10^{-7}$ mbar. Next a flow of gaseous $Ar+N_2$ mixture is established. The dynamic pressure during the sputtering is $3x10^{-3}$ mbar. The electrons emitted by the hot W filaments are accelerated by the electrodes to energies between 40 and 80 eV. An external magnetic field B ≈ 600 Oe is applied parallel to the line connecting the two filaments. The electrons are decelerated and reflected at the opposite gun by the negative potential applied on the filament. Therefore the electrons travel back and forth a few times, ionizing the gaseous mixture, and finally they are absorbed by the grounded electrodes. The result is a ribbon-like low pressure plasma. The plasma has the property that the axial conductivity is high while the transversal conductivity is very low. Therefore, when a transversal electric field is applied in order to extract the ions towards the target or the substrate, the plasma ribbon will stay in position.

As a target we have used metal plates (16mm x 22 mm) with different thickness and composition. In addition, in order to obtain samples with different ratio of metallic elements, the plates were partially covered with Zr wires with a diameter

Table 2.1 Data of the target materials

Target material	Thickness (mm)	Additional elements
Fe	1	-
Fe-25at% Ni-75at%	0.5	-
Fe-99at% Zr-1at%	0.4	-
	0.4	3 Zr wires
	0.4	7 Zr wires
Fe-70at% Co-75at%	2	-
	2	5 Ta chips

Table 2.2 Substrates used for sputter deposition

Substrate type	Thickness (μm)	Top layer
Si (100) or (111)	300	-
Glass	150	-
Si (100)	1000	Si_3N_4
Si(111)	300	Permalloy
Si(100)	1000	Cu
Si(100) or (111)	300	Polymer

of 0.5 mm or Ta chips with a diameter of 2.2 mm as described in the Table 2.1. The samples were deposited on a large variety of substrates which are presented in Table 2.2.

The substrate holder was specially designed in order to facilitate the variation of the deposition temperature between typically -60 to +200°C. The substrates were clamped with a stainless-steel frame against the flat end of the holder, a solid block of Cu, facing the target. The cooling was obtained by bringing the Cu holder in contact with a reservoir containing liquid nitrogen N_2. The high temperatures were obtained by electrical heating.

The influence of the deposition parameters on the magnetic properties of the deposited films will be discussed in the next chapters. It is important to mention here that our sputtering facility enables us to vary all deposition parameters: substrate temperature, pressure during the deposition, gaseous composition, voltage on the target or substrate, etc.

2.1.3. Gaseous treatments

Gaseous nitriding and magnetic annealing were performed in a nitriding furnace presented in Fig. 2.3. The body of the furnace is mainly made of Pyrex glass. No metal parts are used in the heated region. The surface of the sample was exposed at a constant gas mixture which flows continuously due to thermal convection. After the sample was introduced into the cold region of the furnace, the system was flushed first with N_2, evacuated to 2 mbar and then the same procedure was repeated using

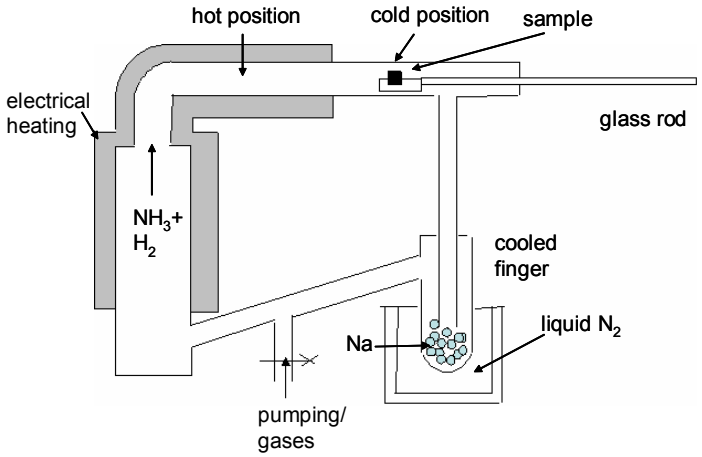

Fig. 2.3 A schematic drawing of the nitriding furnance.

pure H_2. The partial pressures of NH_3 and H_2 gases were calculated in order to ensure a certain nitriding potential $R_N = \ln(P_{NH3}/P_{H2}^{3/2})$, where the pressures are in Pascal). First, NH_3 is introduced in the furnace and trapped in a finger containing Na frozen with liquid nitrogen. The system is filled with H_2 when the total pressure is 2 mbar. After this, the cooled finger is heated to room temperature in order to release NH_3. This procedure gives us the possibility to have a highly accurate control of the partial pressures. We note that the Na has also the role of removing the water or O_2 present in the gas mixture. Next, the sample is moved in the heated region when the total pressure stabilizes. The partial pressures were checked once again after the nitriding was over. It turns out that no significant change in the nitriding potential was found.

2.2. Experimental equipment and principles

2.2.1. X-ray diffraction

A rich variety of information can be extracted from X-ray Diffraction (XRD) measurements. From the position and shape of the lines, one can obtain the unit cell parameters and microstructural parameters (grain size, microstrain, etc.) respectively. By using the flexibility of a four circle diffractometer one can obtain information about the distribution of the orientation of the crystallites (texture measurements).

Standard θ-2θ scans

The geometry of the XRD measurements is depicted in Fig. 2.4. An X-ray beam impinges on a sample and the intensity of the scattered beam is measured.

In order to determine the lattice parameter and the average grain size in our samples we have performed standard θ-2θ scans. The parameters of the diffraction line: position and width were obtained using the fitting program XFIT [2]. In XFIT a de-convolution approach of the X-ray line-profile is used, based on the method developed by Wilson [3] and Klug [4]. Three functions are used in the fitting procedure for the deconvolution of an experimental diffraction line: the emission profile of the radiation (Cu Kα in our case), a function describing the diffractometer broadening and a function containing the physical characteristics of the specimen (average grain size and/ or the micro-strain). We have checked the magnitude of the contribution of the instrument to the broadening of the diffraction lines using Si wafers. We have found that this contribution is much smaller than that of our nanocrystalline samples. Consequently we have assigned the entire broadening of the experimental line to the effect due to the specimen. Usually the lines could be fitted with Lorentzian functions, suggesting that the main contribution to the line-width is due to the reduced size of the crystallites. Under these conditions the observed profile was fitted with a convolution of the emission profile of the Cu Kα radiation and a Lorentzian. The relation between the average crystallite size (CS-in Å) and the full

width at half maximum (FWHM-in rad) of the Lorentzian is given by the Scherrer formula:

$$CS = \frac{\lambda}{FWHM\ cos\,\theta} \tag{2.1}$$

where λ=1.54056Å.

In this approach, we have neglected other sources of the broadening like inhomogenous stress fields. However, we have found a remarkable good agreement between the CS extracted from XRD and direct Transmission Electron Microscopy (TEM) grain size determination [5]. The importance of the XRD technique is due to the fact that by a simple measurement and interpretation we obtain a parameter describing an average property of the microstructure.

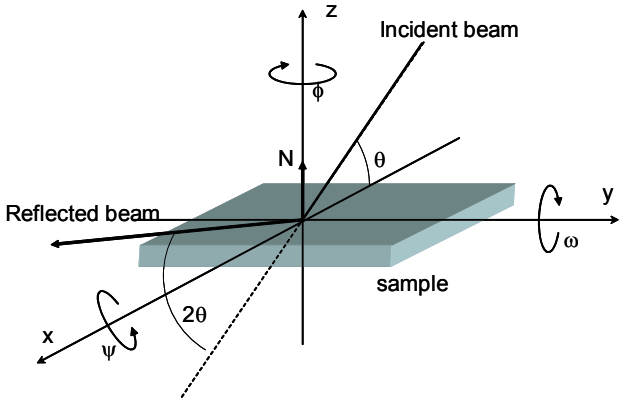

Fig. 2.4 Coordinate system and specific angles for XRD measurements.

Texture measurements are used to determine the preferential orientation of the grains in a polycrystalline sample. The result of a texture measurement can be plotted in a pole figure. This is often represented in polar coordinates consisting of the tilt (ψ) and the rotation (ϕ) angles with respect to a given crystallographic orientation. A pole figure is measured at a constant scattering angle (constant d-spacing) and consists of a series of ϕ-scans (in-plane rotation around the center of the sample) at different tilt ψ -(azimuth) angles (Fig. 2.4). The pole figure data are displayed as contour plots or elevation graphs with zero angle in the center.

The texture measurements were performed using a Philips X-Pert diffractometer.

2.2.2. Mössbauer Spectroscopy

Mössbauer spectroscopy (MS) is used to get information on the local environment of nuclei [6]. In contrast to XRD, it also provides information on compounds that do not exhibit long-range order (poorly crystalline or amorphous materials). The technique is based on the Mössbauer effect, i.e. for nuclei placed in a solid there is a certain probability that the emission or absorption of a γ-ray photon takes place recoilless, i.e. without absorption or emission of a photon. For the MS measurements presented in this work we used absorption into and emission from the first excited state at 14.4 keV of the stable isotope ^{57}Fe. The energy distribution of the emitted radiation can be approximated by a Lorentzian with a FWHM of 4.7 10^{-9} eV. In iron at room temperature the recoilless fraction is of the order of 0.80. For the samples investigated in this thesis the ^{57}Fe isotope is present in its natural abundance, i.e. 2%. In the case of ^{57}Fe spectroscopy the recoilless 14.4 keV gamma rays are emitted by an excited ^{57}Fe nucleus obtained from the decay of its parent ^{57}Co (half life = 270 days). The radioactive ^{57}Co atoms are embedded in a cubic matrix (Rh) to ensure the emission of a single photon energy. The γ quanta are resonantly absorbed by the ^{57}Fe atoms present in the sample to be investigated. However, due to interaction between the nucleus and the surrounding electrons (hyperfine interactions) small shifts or splittings of the nuclear levels in the absorber are present. The so-called isomer shift reflects the fact that the energy of the nucleus depends on the electron density at the nucleus and the energy shift is different for the ground and excited states. The shift depends on the environment of the nucleus and thus on the type of material. A splitting arises by the interaction between the quadrupole moment of the nucleus and the gradient of the electric field at the nucleus caused by the surrounding electrons (quadrupole interaction) or through the coupling between the nuclear magnetic moment and the magnetic field at the nucleus (magnetic hyperfine interaction – Zeeman splitting). The shift and/ or splitting due to these hyperfine interactions are larger than the natural line width of the 14.4 keV line. However, they are of the same order of magnitude as shifts in the γ-ray energy that can be introduced via the Doppler effect by moving the emitter with respect to the absorber. By measuring the resonant absorption as a function of the relative velocity a Mössbauer spectrum is created. The hyperfine parameters: isomer shift, quadrupole splitting and hyperfine field can be extracted from the experimental spectra, taking into account the emission spectrum of the source which consists of a single line. By comparing with the tabulated data, the environment of the absorbing atom can be determined. Often nuclei in the sample have different surroundings leading to a complicated spectrum which has to be decomposed. The spectra presented in this work were analyzed using a computer code (MCTL) developed in our laboratory.

The Mössbauer spectra were obtained using a constant acceleration spectrometer in conjunction with a 1024 multichannel analyzer and a 20mCi radioactive ^{57}Co(Rh) source. The foils were measured in the transmission mode. In

this mode the γ-rays transmitted trough the sample are counted and the recoilless absorption is observed as dips in the spectrum. The thin sputter deposited layers were measured by a technique called Conversion Electron Mössbauer Spectroscopy (CEMS). In this technique the electrons emitted by internal conversion during the decay of the excited absorber nuclei are recorded. The recoilless absorption is revealed as peaks in the spectrum.

2.2.3. Rutherford backscattering spectroscopy

Rutherford backscattering (RBS) is a technique used for the analysis of materials in order to determine the depth distribution of the elements in a given sample [7]. Usually RBS is used for depth profiling of heavy atoms (Z>10). In RBS a beam of H^+ or He^+ ions, with typical energies in the 1-4 MeV range, bombards the sample. The beam particles backscattered from the sample are detected and their energy is analyzed. The interaction between an ion from the beam and an atom from the sample, in the energy range used, is governed by the Coulomb repulsion between two nuclei. The energy transfer between the particles in this elastic collision is calculated by applying the principles of conservation of energy and momentum. While traveling through the sample the beam particles experience an energy loss due to inelastic collisions with the electrons in the sample. For ions with energies in the keV range or higher the deflection and the electronic collisions can be treated as separate problems. An additional approximation is usually applied in the RBS analysis: the single scattering approximation. In this approximation is assumed that an ion arriving in the detector has undergone only one large-angle scattering. Since the propagation of the ion is hardly affected by the collisions with the electrons, the trajectories of the ions can be considered straight to a good approximation. Based on this approximation the following calculations can be made:

- the ratio of the energies of the backscattered particle after and before the collision is given by the kinematic factor and it is determined by the mass ratio of the projectile and target atoms and the scattering angle.
- the yield of the backscattering atoms is proportional to the Rutherford cross-section. The yield can be then related to the areal density (atoms per unit area) of the elements in the sample.
- using tabulated values for the energy and loss of the ions, the energy scale can be translated into a depth scale for each element.

Near the surface (5nm) the depth resolution is determined by the energy resolution of the detector. Depending on ion species, energy and resolution, the depth profiling is possible for ranges extending up to few micrometers. The Si detectors used in this work have an energy resolution of 15keV, yielding a depth resolution of about 50Å for a backscattering angle of 165°. At larger depths, the resolution decreases by the straggling effect. Straggling occurs as a result of the statistical

distribution in the number of interactions experienced by the incoming and outgoing particles inside the target.

In the present investigations RBS measurements were done in a high-vacuum chamber with a base pressure better than 10^{-8}mbar. A He^{+} beam with energy between 1 and 2 MeV was used. The backscattered ions were detected simultaneously with three silicon barrier detectors at 105, 135 and 165° scattering angles. The samples were mounted in a two axis goniometer with long range reproducibility and accuracy of better than 0.1°. Additionally, the sample holder can perform translation movements in two perpendicular directions in steps of 0.1 mm. This facility was used for the detection of the lateral distribution of the thickness of the sputtered samples. The complete analysis of the RBS spectra was performed using the computer program "Nuclear Data Furnance" (NDF) developed at the University of Surrey [8, 9].

2.2.4. Transmission electron microscopy

Transmission Electron Microscopy (TEM) is a versatile tool capable of characterizing the internal structure of a wide variety of materials [10]. This characterization includes not only the imaging of the microstructure directly but at the same time, the identification of the phases present in the specimen by either electron diffraction or spectroscopic chemical analysis. The results obtained from a typical TEM characterization of materials allow a better understanding of the relation between microstructure and properties.

There is a rich variety of operation modes of the electron microscope. The Bright Field (BF) mode is commonly used to image grain and defect structures within materials. It can also reveal second phases such as precipitates and inclusions. Similar in purpose to the BF technique, the Dark Field (DF) imaging mode makes use of the specific Bragg diffracted electrons to image the region from which they originate. The DF mode enables the link between the crystallographic information and specific regions or phases in the sample. The primary purpose of the electron diffraction technique is to identify the crystal structure of the materials under investigation. By placing an aperture in the image plane, then projecting the diffraction pattern of that image onto recording plate, one obtains the Selected Area Diffraction technique. Using the technique called Lorentz Microscopy it is possible to obtain images with the contrast given by the variation of the direction of the magnetization in the specimen. Most of the TEM characterization experiments are performed on static structures. However the modern microscopes have the capability to observe structures under dynamic conditions. Using an in-situ heating unit ($T<800$ K) the evolution of the morphology of the sample during the thermal treatment can be monitored.

2.2.5. Scanning probe microscopy

Scanning probe microscopy (SPM) [11] represents a group of techniques oriented towards investigation of the materials surface. The principle of SPM is based on scanning of the surface with a sharp probe, revealing information regarding various physical properties from atomic to micrometer level. The detection is performed measuring the cantilever deflection using a laser beam which is reflected by the back side on a position sensitive photo-detector. In our work we have used two SPM techniques: Atomic Force Microscopy (AFM) to reveal surface topography and Magnetic Force Microscopy (MFM) for imaging the magnetic structure.

We have chosen for our samples the taping mode AFM. In this mode a cantilever is oscillated at its resonant frequency and scanned across the sample surface. Typical amplitudes of oscillations are 20-100 nm. The amplitude is changing when the tip scans over bumps and depressions on the surface. The advantages of this scanning mode are: i) high lateral resolution (1-5nm), ii) lower forces and less damage to the soft samples imaged in air and iii) lateral forces are virtually eliminated.

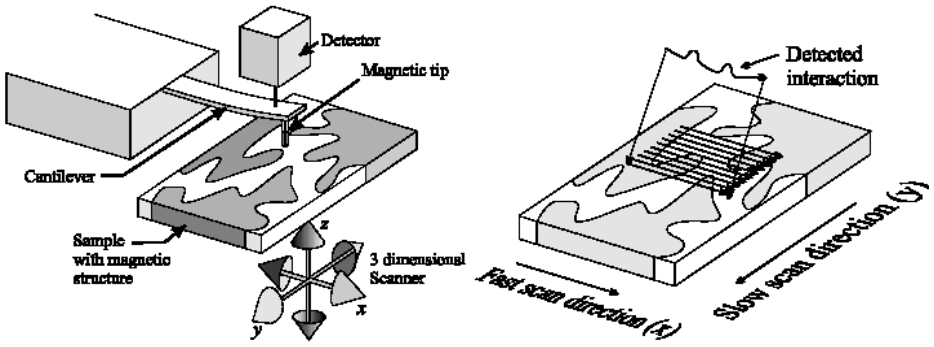

Fig. 2.5 Basic principle of Magnetic Force Microscopy [12]

In Fig. 2.5 we present the MFM principle. The characteristic feature of this technique is that a tip covered with a thin magnetic film interacts with the sample surface via the magnetic stray fields of the sample. The distance between the tip and the surface is 10-100nm. In order to image the magnetic structure the amplitude, the frequency and the phase are monitored.

2.2.6. Vibrating sample magnetometry

A popular method for determining the magnetic properties of a wide variety of magnetic systems is vibrating sample magnetometry. With this technique the magnetic moment of a sample can be measured with a high accuracy. The

measurements can be performed in a DC external field. Some of the Vibrating Sample Magnetometers (VSM) have also the facility of measuring the magnetic moment at different temperatures increasing even more the area of investigations. In our work, room temperature measurements of hysteresis loops were performed on a regular basis in order to establish the suitability of a certain production method for our objectives and to contribute to understanding of the magnetic permeability behavior at high frequencies.

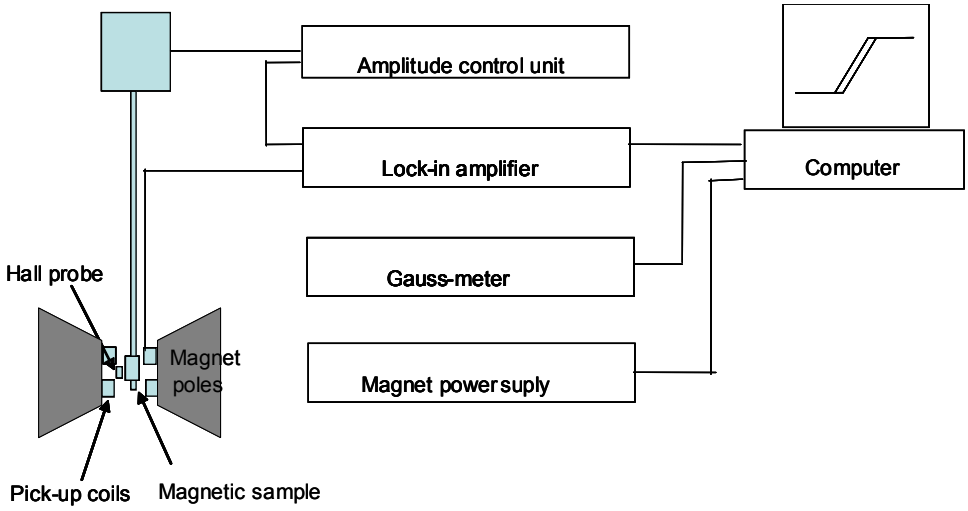

Fig. 2.6 Block diagram of the VSM

A schematic representation of the VSM used in our research is given in Fig. 2.6. The magnetization of the sample creates a magnetic stray field which is frequency modulated by vibrating the sample. As the sample is situated between a pair of pick-up coils, an AC voltage with the same frequency and proportional to the sample magnetization is induced in the coils. A lock-in amplifier is used to provide the frequency of vibrations and to detect the signal. Special attention was given to obtain constant amplitude of the oscillations over the time interval specific to our measurements. The system is calibrated with a magnetic material with a known saturation magnetization, e.g. Ni. A Hall probe was used in order to determine the values of the applied field. Using the computer interface, the magnetic field and the signal proportional to the magnetic moment can be simultaneously recorded (hysteresis loops). The sensitivity of the instrument was sufficient to measure hysteresis loops of Fe samples with a thickness of only 10nm. It is important to mention that the absolute values of the saturation magnetization can be determined only if the density and the amount of magnetic material are precisely known

(M_S=magnetic moment/ sample volume). For very thin films this can be a difficult task.

2.2.7. Torque magnetometry

The principle of a torque magnetometer is based on the fact that a sample in a magnetic field experiences a force. The torque exerted on a sample is proportional to its magnetization and also to the derivative of the anisotropy energy towards the angle of rotation. We present in Fig. 2.7 a simplified drawing of the torque set-up used by us. A sample-holder with a sample hanging on a thin wire is shown. At the top end of the sample-holder, a coil is mounted between a permanent magnet of a known strength. The torque on the sample can now be compensated by a torque on the coil when a current flows through this coil. Using a small mirror, a lamp and two photo diodes to detect the rotation of the sample, the current through the compensation coil is controlled.

The current through the compensation coil is proportional to the torque exerted on the sample. Torque magnetometers are often used for determining the anisotropy (preferential magnetisation) axis in a magnetic material.

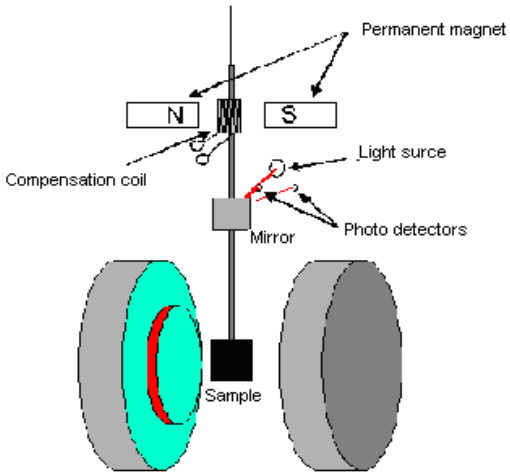

Fig. 2.7 Torque magnetometer set-up.

One of the major problems in torque magnetometry is the fact that the anisotropy energy is determined by the angle between the magnetization (**M**) and the easy axis direction (α) whereas we set the angle between the applied field (**H**) and the easy axis (φ). The magnetization direction is free to rotate to the equilibrium position where the torque exerted by the applied field balances the torque exerted by the anisotropy. Therefore α and φ are not equal, see Fig. 2.8. Under these conditions, there are two possibilities to evaluate the torque given by the anisotropy. One is to calculate α for every φ using the value of **M** measured with a different technique. The second approach is to take torque measurements at many different values of **H** and to extrapolate the measurement value to the infinite field. Very often the anisotropy values obtained by both methods are very different. One of the major reasons for this is the non-uniformity of the anisotropy. Since the non-uniformity in the anisotropy is unknown beforehand, the extrapolation method is to be preferred.

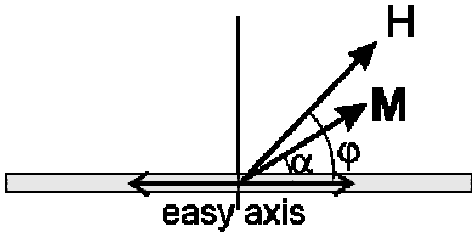

Fig. 2.8 The orientation of **M** and **H** the when the rotation axis is in the plane of the sample; the sample is oriented perpendicular to the plane of paper.

2.2.8. Field dependent ferromagnetic resonance

Ferromagnetic Resonance (*FMR*) is a technique which is used for study of the magnetization dynamics in thin films and bulk materials. Valuable information regarding anisotropy and saturation magnetization can be also obtained. The principle consists in measuring the absorbed power of a microwave field applied perpendicular to the direction of the magnetization. We obtain maximum coupling between the RF field and the spin system when the frequency ω_{RF} of the incident power is equal to the frequency of the spins precession ω_L given by the effective field on the sample. To the effective field contribute all magnetic interactions that exert a torque on the spin system. A description of fields and magnetization orientation is presented in Fig. 2.9.

In standard *FMR*, ω_{RF} is kept constant and an external DC field is swept in order to mach ω_L. These are so called field dependent *FMR* experiments [13] and can be performed with commercial Electron Spin Resonance (ESR) spectrometers. The RF power (about 2mW) generated by a klystron is applied to the sample placed in a resonance cavity. The absorbed power can be measured by means of lock-in detection techniques and plotted against the values of the external DC field. Because the line intensity is given in arbitrary units a quantitative estimation of the complex permeability is not possible. A goniometer with the rotation axis perpendicular to the applied field allows angle-dependent measurements. This was used for determining the magnetic anisotropy field. One of the great advantages of the field dependent FMR is that we can determine the saturation magnetization, regardless the sample volume. The error bar reduces to just 2-3%. See section 4.4.1. of Chapter 4 for more details.

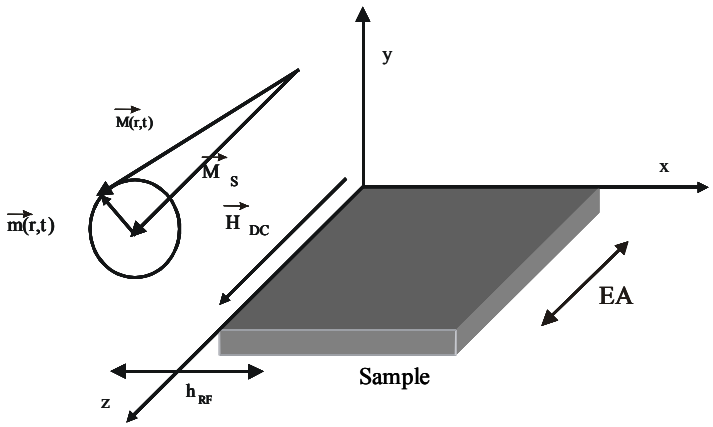

Fig. 2.9 Magnetization and field orientation.

2.2.9. High frequency magnetic permeability

In order to demonstrate that a certain ferromagnetic material is suitable for high frequency applications it is necessary to have reliable measurements of magnetic permeability over a large frequency range. Different broad band techniques were developed in the last 10 years. Permeameters based on two ports [14, 15] or a single port [16, 17] were produced as part of diverse research projects. Depending on the shape of the material a certain method can be chosen. For instance, permeability

measurements in the 50MHz-18GHz range were reported for flexible ferromagnetic ribbons or wires [18]. In this case the measurement device consists of a *coaxial* transmission line in which a toroid obtained by bending the ribbons or the wires was inserted. Such geometry is not suited for the material presented here. We have used a single port device in order to measure the permeability of our thin films at a constant external field. The present design operates up to 6GHz [19]. In the following part we present the details of this technique developed in our laboratory.

Experimental set-up

The measurement device is based on a copper single coil designed to ensure the best matching with a transmission line having a characteristic impedance of 50Ω, see Fig. 2.10. Using an Impedance Analyzer (from 1MHz to 1.8GHz) or a Network Analyzer (from 130MHz to 5.5 GHz) the reflection parameter S_{11} of the single coil device is measured. Prior to this, the reference Π plane has to be determined in order to make a proper correction for the electrical length (S_{11}=-1). This operation is required in order to take into account the extra length added due to the device connector. The impedance is then obtained from the expression:

$$Z_m = Z_0 \frac{1+S_{11}}{1-S_{11}} \tag{2.2}$$

where $|S_{11}|^2$= power reflected from the network input/ power incident on the network input, Z_0 is the characteristic impedance of the transmission line (ended at the Π plane).

The samples are deposited on 0.2 ÷ 0.3 mm thick substrates with an area of 4.5x4.5mm. We have chosen these dimensions in order to have a homogenous RF field acting on the sample. The direction of the RF field will coincide with the axis of the coil. Important to mention is the nature of the substrate because we observed that glass and Si(100) give different RF responses, probably due to slightly different dielectric properties. Even more, we have measured different RF responses for the same Si(100) substrate which was treated at different temperatures. Therefore the thinner the substrate the less "parasite" effects due to the substrate are present in the total measured impedance.

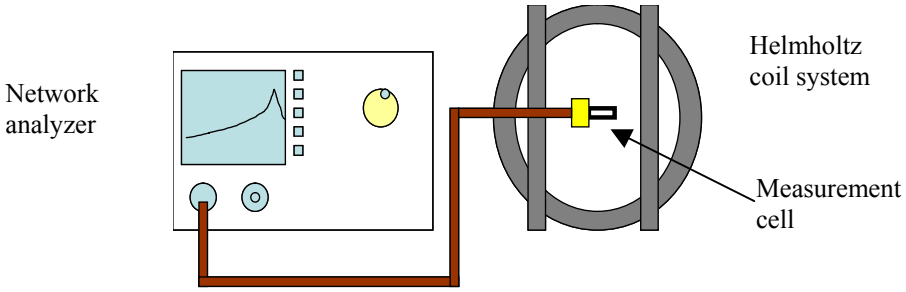

Fig. 2.10 Permeability measurement set-up. Two Helmholtz coils are used in order to align the magnetization parallel and perpendicular to the RF field.

Equivalent circuit interpretation

The analysis consists of an evaluation of the magnetic flux perturbation when the ferromagnetic film is introduced into the coil. The microwave field can be considered as:

$$h = \frac{ki}{W} \tag{2.3}$$

where $i=i_0 exp(-j\omega t)$ is the high frequency current, k is the calibration constant (which has to be determined using a known sample) and W is the length of the device. By inserting the magnetic material into the cell the variation in magnetic flux will be:

$$\Delta\phi = \mu_0(\mu_r - 1)hW_S t_S \tag{2.4}$$

with t_S, W_S the thickness and width respectively, of the magnetic thin film. Applying Faraday's law the complex change in voltage at the coil entry is given by:

$$\Delta v = j\omega\mu_0(\mu_r - 1)hW_S t_S \tag{2.5}$$

Substituting the high frequency field from Eq. 2.3 the coil impedance induced by the flux $\Delta\phi$ is:

$$\Delta Z = \frac{\Delta v}{i} = j\omega\mu_0(\mu_r - 1)k\frac{W_S}{W}t_S \tag{2.6}$$

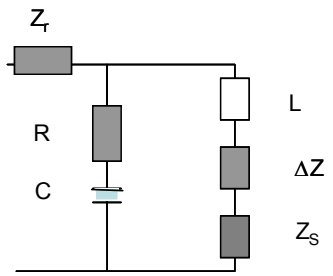

Fig. 2.11 Equivalent electrical circuit of the measurement cell; ΔZ is the change in impedance due to magnetic material, Z_S is the impedance of the substrate and Z_r is the residual impedance.

The direct determination of ΔZ and the determination of the passive elements constituting the equivalent circuit of the measuring device (see Fig. 2.11) lead to the calculated values of the permeability. It should be noted that the measurement device has a more complicated behavior as a function of frequency and the equivalent lumped circuit used here is just an approximation of the real physical system within the frequency range of interest. Consequently we have introduced an extra element Z_r in the analysis of the measuring device to account for the effects which can not be described by a passive circuit element. This complex residual impedance Z_r has to be calculated for each frequency (see next section). Measurements of the complex permeability using this type of analysis performed on the same sample but using measurement devices with different parameters lead to the same results. Z_r may be associated with the parasitic impedance supposed to exist at the joint between the transmission line and the strip coil. In the next section we discuss how we obtain the parameters of the equivalent circuit.

Calculation of the magnetic permeability

Next we present the steps required in order to obtain the complex permeability response.

a) The impedance curve corresponding to the empty cell is fitted according to the following analytical expression:

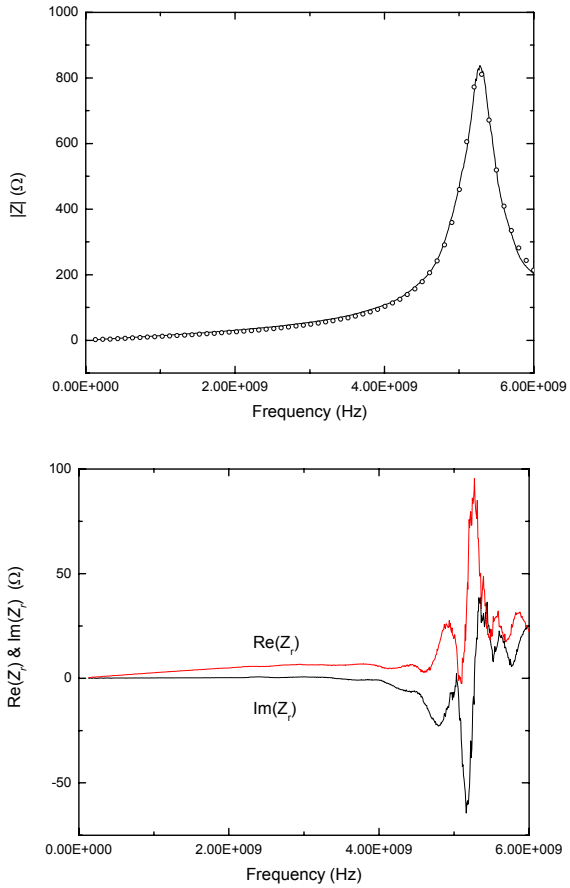

Fig. 2.12 a) Impedance of the empty measurement cell: the line corresponds to the measurement and the dots are the fit with Eq. (2.7); b) Real and imaginary part of residual impedance.

$$Z_m = \frac{\left(R + \frac{1}{j\omega C}\right)\left(Z_S + \Delta Z + j\omega L\right)}{R + \frac{1}{j\omega C} + j\omega L + Z_S + \Delta Z} \tag{2.7}$$

For the empty cell, ΔZ and the substrate impedance Z_S are 0 and the fitting parameters are R, L and C. We can see in Fig. 2.12a that the fit reproduces the experimental data reasonably well. The number of points corresponding to the frequency interval of interest has to be maximized in order to improve the statistics.
Using the values of R, L and C obtained at step (a) we calculate $Z_r=Z_r(f)$ from the impedance spectra of the empty cell. This is done by subtracting the calculated spectra from the experimental one. These values will be further subtracted from the impedance spectra corresponding to the cell loaded with the substrate and the cell loaded with substrate plus magnetic thin film. Although Z_r is much smaller than Z_m, its magnitude is comparable with $\Delta Z=\Delta Z(f)$. Note that the frequency range over which we compare these spectra must be below the resonance frequency of the cell.

c) The values of Z_S are calculated using Eq. (2.7) and taking into account Z_r. In this case we can measure Z_m either when we insert a bare substrate with exact size like the sample or when the magnetization is oriented parallel to the high frequency field. For reasons of system stability we prefer the second alternative.

d) Calculate μ_r on the basis of Eq. (2.6) and the following formula derived from Eq. (2.7):

$$\Delta Z = \frac{\left(R + \frac{1}{j\omega C}\right)\left(Z_S + j\omega L\right) - Z_m\left(R + \frac{1}{j\omega C} + j\omega L + Z_S\right)}{Z_m - R - \frac{1}{j\omega C}} \tag{2.8}$$

In Fig. 2.13 we present as an example the permeability spectra of a Fe-Co-Ta-N sample measured in zero applied field.

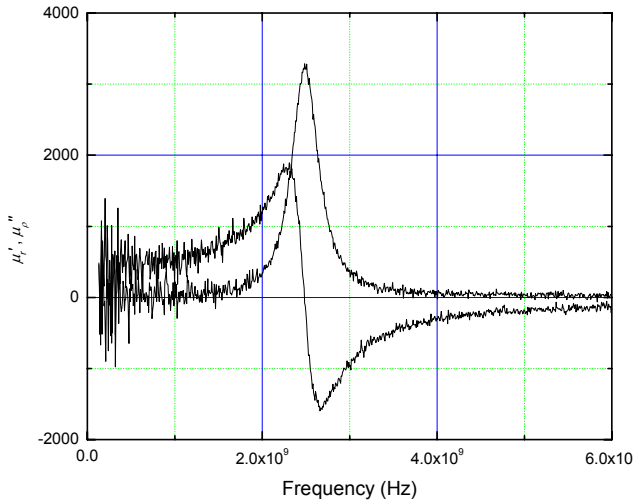

Fig. 2.13. Permeability spectra obtained using the method presented in this section.

References

1. P. J. Kelly and R. D. Arnell, Vacuum **56,** 159 (2000).
2. R. W. Cheary and A. Coehlo, J. Appl. Cryst. **25,** 109 (1992).
3. A. J. C. Wilson, Mathematical Theory of X-ray Powder Diffractometry, 1963, New York: Gordon and Breach.
4. H. P. Klug and L. E. Alexander, X-ray Diffraction Procedures, 2nd ed., New York: Wiley-Interscience, 1964.
5. A.R. Chezan, thesis (Groningen, 2002) chapter 5.
6. N. N. Greenwood and T. C. Gibb, Mössbauer Spectroscopy, Chapman and Hall, London, 1971.
7. Handbook of modern ion beam materials analysis, Ed. J. R. Tesma, M. Nastasi, J. C. Barbow, C. J. Maggiore, J.W. Mayer, Materials Research Society, Pittsburg, PA, 1995.
8. N. P. Barradas, C. Jeynes and R. P. Webb, Appl. Phys. Lett.**71,** 291 (1997).
9. N. P. Barradas, K. P. Marriott, C. Jeynes and R. P. Webb, Nucl. Instr. and Meth.B, **136-138,** 1157 (1998).
10. D. B. Williams and C. B. Carter, Transmission electron microscopy: a textbook for materials science, Plenum Press, New York, 1996.
11. R. Wiesendanger, Scanning Probe Microscopy: Methods and Applications, Cambridge University Press, 1994.
12. S. Porthun, L. Abelmann, S.J.L. Vellekoop, J.C. Lodder, H.I. Hug, JMMM, **182,** 238 (1998).
13. C. Vittoria, Microwave properties of magnetic films, World scientific, 1993.
14. V. Cagan and M. Guyot, IEEE Trans. Mag. MAG-**20,** 1732 (1984).
15. C. A. Grimes, P. L. Prodan, J. Appl. Phys. **73,** 6989 (1993).
16. J. C. Peuzin and J. C. Gay, Acte de Journees de l'études sur la characterisation microonde des materiaux absorbants, Limoges 75 (1991).
17. A. Fessant, J. Gieraltowski, J. Loaec, H. Le Gall, and A. Rakii, IEEE Trans. Magn. **29**, 82 (1993).
18. O. Acher, J. L.Vermeulen, P. M. Jacquart, J. M. Fontaine, and P. Baclet, J. Magn. Magn. Mater. **136,** 269 (1994).
19. D. Pain, M. Ledieu, O. Acher, A. C. Adenot, and F. Duverger, J. Appl. Phys. **85**, 5151 (1999).